BULLETIN OF THE POLISH ACADEMY OF SCIENCES
TECHNICAL SCIENCES, Vol. 74(1), 2026, Article number: e155900
DOI: 10.24425/bpasts.2025.155900

On compliance minimization by biomimetic regularization method

Michał NOWAK[1,2]*, **Jan SOKOŁOWSKI**[2], **Antoni ŻOCHOWSKI**[2], **and Jan POLAK**[1]

[1] Poznan University of Technology, ul. J. Rychlewskiego 1, 61-131 Poznań, Poland
[2] Systems Research Institute of the Polish Academy of Sciences, ul. Newelska 6, 01-447 Warszawa, Poland

Abstract. The standard approach to mechanical design is based on strength hypotheses. However, the structural optimization methods do not take into account this important condition determining the correctness of the engineering solution. The situation is different in the case of biological systems, where reference to material strength is a basic condition for the formation of functional mechanically loaded systems. The team developed an optimization system modeled on the phenomenon of bone remodeling, based on rigorous theoretical studies in the field of material continuum optimization, where the condition for achieving the optimal solution is the equalization of strain energy density on the structural surface. The new idea presented in this paper is to link this condition with the strength properties of the material. Furthermore the strength hypotheses are expressed in terms of strain energy. The aim of the research presented in this paper is to precisely estimate the relationship between the condition of a constant value of the strain energy density on the structural surface and the material strength, according to yield criteria. The given numerical examples contain a reference to the analytical results and indicate a unique feature of the presented method. The use of the notion of insensitivity zone concept for building the biomimetic structural optimization system allows regularization without focusing on the existence of the Lagrange multiplier correspondence to the volume constraint. The approach presented in the paper can be used by engineers as a method for structural optimization no longer bound to the phenomenon of trabecular bone remodeling. Also discussed is the problem of numerical implementation and the necessary modification of the position and size of the insensitivity zone to ensure that the result is achieved by numerical means. These results require the development of appropriate heuristics but allow us to achieve similar results regardless of the initial configuration. However, the discussion of the use of observations of Nature in mechanical design remains open.

Keywords: mechanical design; free boundary problem; biomimetic structural optimization; shape optimization; optimality conditions; trabecular bone remodeling.

1. INTRODUCTION

1.1. A free boundary problem

The shape and topology optimizations in structural mechanics are a relatively new domain within scientific computing. Such problems are nonconvex and ill-posed in general.

In mathematical setting, the nonexistence of optimal shapes usually requires the appropriate regularization technique [1]. The convergence of numerical methods for solution of gradient flow dynamical systems is still under construction, we refer the reader to [1] for a review of available results. In our case, the results are presented under assumption that an optimal shape does exist. The necessary optimality condition for the compliance optimization leads to a nonlinear boundary condition on the moving boundary. Thus, the shape and topology optimization problem could be considered as a free boundary problem for elasticity. To our best knowledge such a free boundary value problem has not been considered yet in the literature. The convergence of the gradient flow dynamical system for scalar problems is shown at the continuous level in the forthcoming book by Plotnikov and Sokolowski.

*e-mail: michal.nowak@put.poznan.pl

Manuscript submitted 2025-08-13, revised 2025-09-17, initially accepted for publication 2025-09-30, published in January 2026.

In the paper a numerical method is proposed and tested for a free boundary problem in elasticity. We denote by Ω an elastic body. A part of its boundary $\Gamma \subset \partial\Omega$ is unknown along with a constant λ and should be determined together with the displacement vector field u, deformation tensor field $\varepsilon(u)$ and the stress tensor field $\sigma(u)$. Let n stand for the unitary exterior normal field on $\partial\Omega$ and the traction vector field $P := \sigma \cdot n$ be defined on the boundary of elastic body. Free boundary problem is defined by imposing two conditions on unknown free boundary Γ

$$P = \sigma(u) \cdot n = 0, \sigma(u) : \varepsilon(u) = \lambda,$$

where $\lambda \in \mathbb{R}$ is unknown constant and it should be determined along with the free boundary and the solution of the elasticity system. In other words the free boundary is traction-free and the elastic energy is constant on the free boundary. Such a free boundary problem arises in shape and topology optimization for compliance with the volume constraints. Using the necessary optimality conditions for the compliance minimization, the constant λ can be considered as a Lagrangian multiplier for the volume constraints. In the paper we present a new method of its a priori evaluation, which considerably simplifies the numerical method. The piece of the boundary Γ is assumed to be traction-free. In order to solve the free boundary problem the functional shape is minimized with respect to traction free Γ. The main

difficulty to use the method is the necessity to find the multiplier λ. We propose the method of its determination by careful examination of material properties, which seems to be original contribution of the paper. In addition, our method allows for direct manufacturing of obtained shape by using the additive manufacturing techniques with 3D printers [2–4]. This means that an optimum design obtained by our method is not singular from the point of view of practical applications in structural optimization.

From mathematical point of view there are few questions addressed for the nonconvex shape and topology optimization problem under consideration. The first is if the problem is well posed from mathematical point of view, i.e., there is an optimal solution which continuously depends on the data. The answer is usually negative and an appropriate regularization technique is required. The geometric regularization is appropriate and it could also lead to the convergence of the gradient flow dynamic system to an optimal shape, we refer to the first result in this direction [1]. Let us also recall that the variable insensitive zone in our numerical method is conceptually related to the shifted penalty function, see, e.g., [5, 6].

1.2. Optimum design in elasticity

The standard approach to mechanical design is based on strength hypotheses. During the design of a mechanical structure, it is necessary to shape it in such a way that the material subjected to multidirectional loads will not be damaged. To determine whether such damage will occur, damage criteria are used, usually related to the stresses present in the structure. Already in the 17th century Hook began studying the concepts of elasticity theory. However, it was not until the 19th century, with the emergence of continuum mechanics that the concept of the failure criterion could be considered. Many concepts and theories have been developed based on the mechanics of continuous media, and different assumptions and experimental results have led to the development of different failure criteria [7–9]. Currently, the most commonly used criterion (especially in commercial computational systems using the finite element method) is the Huber-Mises-Hencky criterion. According to the Huber-Mises-Hencky theory, the evaluation of the allowable stress of a structure can be performed by determining the maximum distortion strain energy (deviatoric strain energy). This theory allows for the calculation of the so-called von Mises stress, which is not a true stress, but a theoretical value that allows the comparison of any spatial stress state with the uniaxial yield stress. According to the maximum distortion energy theory, yielding occurs when the distortion energy reaches this critical value. The critical value of distortion energy, which is material-specific, can be obtained experimentally through a simple tension test. In this way, universal design guidelines can be obtained for a specific material, regardless of the loading state of the entire analyzed structure. Therefore, when performing structural optimization assuming the use of a specific material, the optimal solution differs depending on the material. Therefore, the idea naturally arises to experimentally investigate the critical value for a specific material and take it as the starting point of the optimization procedure. The team developed an optimization system modeled on the phenomenon of bone remodeling, based on rigorous theoretical studies in the field of material continuum optimization, where the condition for achieving the optimal solution is the equalization of strain energy density on the structural surface. Furthermore the strength hypotheses are expressed in terms of strain energy. The aim of the research presented in this paper is to precisely estimate the relationship between the condition of a constant value of the strain energy density on the structural surface and the material strength, according to yield criteria. Such a discussion can be conducted for various criteria. This paper focuses on two such criteria that are commonly used in mechanical design. The Huber-Mises-Hencky criterion and the Tresca criterion, which may prove important when the discussion is extended to uncertainty analysis [10].

2. BIOMIMETIC STRUCTURAL OPTIMIZATION METHOD – THE STIFFEST DESIGN

The method used in the paper is based on the observation of adaptive remodeling of trabecular bone. The starting point is a precise theoretical result concerning the stiffest design problem. So, the goal is to maximize the stiffness of a structure, that is minimization of the functional

$$J(\Omega) = \int_{\Gamma_1} \mathbf{t}.\mathbf{u}\,\mathrm{d}s \tag{1}$$

under constraints

$$\int_{\Omega} \mathrm{d}x - V_0 = 0 \tag{2}$$

and state equations

$$\mathbf{div}\,\boldsymbol{\sigma}(\mathbf{u}) = 0 \quad \text{in} \quad \Omega, \tag{3}$$

$$\boldsymbol{\sigma}(\mathbf{u}).\mathbf{n} = \mathbf{t} \quad \text{on} \quad \Gamma_1, \tag{4}$$

$$\boldsymbol{\sigma}(\mathbf{u}).\mathbf{n} = 0 \quad \text{on} \quad \Gamma_v, \tag{5}$$

$$\mathbf{u} = 0 \quad \text{on} \quad \Gamma_0. \tag{6}$$

Here, Ω represents domain of the elasticity system, $\mathbf{u}$ the displacement, $V_0 = |\Omega_0|$ a given volume, Γ_0 part of the boundary with Dirichlet condition, Γ_1 part of the boundary loaded by traction forces, Γ_v part of the boundary subject to modification.

$\partial\Omega = \Gamma_0 \cup \Gamma_1 \cup \Gamma_v$, $\mathbf{t}$ is a constant vector of traction forces and Γ_v is a part of the boundary subject to modification.

The Lagrange function for the problem under consideration can be defined as follows

$$L(\Omega_t, \lambda) = \int_{\Gamma_1} \mathbf{t}.\mathbf{u}_t\,\mathrm{d}s + \lambda \left[\int_{\Omega_t} \mathrm{d}x - V_0 \right]. \tag{7}$$

The state equation in the weak form can be written as follows

$$-\int_{\Omega_t} \boldsymbol{\sigma}(\mathbf{u}_t) : \boldsymbol{\varepsilon}(\boldsymbol{\varphi})\,\mathrm{d}x + \int_{\Gamma_1} \mathbf{t}.\boldsymbol{\varphi}\,\mathrm{d}s = 0. \tag{8}$$

Here $\mathbf{u}_t, \boldsymbol{\varphi} \in \mathbf{H}^1_{\Gamma_0}(\Omega_t)$ and $\Omega_t = T_t(\Omega)$. For fixed field $\mathbf{V}(\mathbf{x})$ which vanishes on the entire boundary of $\partial\Omega$ with the exception of Γ_v, the Lagrange function depends only on two scalar variables (t, λ). Then we take shape derivative of both Lagrange function and weak state equation using speed method. At the local minimum this first derivative should vanish. The shape derivative is denoted here by $(\bullet)'$.

$$[L(\Omega,\lambda)]' = \int_{\Gamma_1} \mathbf{t}.\mathbf{u}'\,\mathrm{d}s + \lambda \int_{\Gamma_v} \mathbf{V}.\mathbf{n}\,\mathrm{d}s = 0, \tag{9}$$

$$-\int_{\Omega} \boldsymbol{\sigma}(\mathbf{u}') : \boldsymbol{\varepsilon}(\boldsymbol{\varphi})\,\mathrm{d}x - \int_{\Gamma_v} \boldsymbol{\sigma}(\mathbf{u}) : \boldsymbol{\varepsilon}(\boldsymbol{\varphi})\mathbf{V}.\mathbf{n}\,\mathrm{d}s = 0. \tag{10}$$

After substituting $\boldsymbol{\varphi} := \mathbf{u}'$ in the weak state equation and $\boldsymbol{\varphi} := \mathbf{u}$ in its shape derivative

$$\int_{\Gamma_1} \mathbf{t}.\mathbf{u}'\,\mathrm{d}s = -\int_{\Gamma_v} \boldsymbol{\sigma}(\mathbf{u}) : \boldsymbol{\varepsilon}(\mathbf{u})\mathbf{V}.\mathbf{n}\,\mathrm{d}s. \tag{11}$$

Using this result in the derivative of Lagrange function gives

$$\int_{\Gamma_v} [\lambda - \boldsymbol{\sigma}(\mathbf{u}) : \boldsymbol{\varepsilon}(\mathbf{u})]\mathbf{V}.\mathbf{n}\,\mathrm{d}s = 0. \tag{12}$$

Since at the stationary point this should hold for any vector field $\mathbf{V}(\mathbf{x})$ on Γ_v, then

$$\boldsymbol{\sigma}(\mathbf{u}) : \boldsymbol{\varepsilon}(\mathbf{u}) = \lambda = \text{const}. \tag{13}$$

For the stiffest design the strain energy density on the part of the boundary subject to modification should be constant. The obtained result, consistent with previous studies [11, 12] and other results [13] can be used to develop a structural optimization method suitable for finding a solution in the form of a structure with minimal mass, with assumed properties related to the material from which the structure is to be made. The assumption concerning the value of the Lagrange multiplier on the surface can be treated interchangeably with the assumed volume condition [14]. Therefore, it is necessary to develop an appropriate algorithm that would implement the postulate of equalizing the energy density on the surface of the structure. Such an algorithm can be found in the phenomenon of adaptive remodeling of trabecular bone.

3. BIOMIMETIC STRUCTURAL OPTIMIZATION METHOD BASED ON TRABECULAR BONE HOMEOSTASIS PRINCIPLE

The first observation of the behaviour of the trabecular bone tissue was made by Wolff and published in 1892 [15]. The observation proposed by Julius Wolff – known as the Wolff's law – can be described as a structural adaptation of the bone to the external forces and is called trabecular bone remodeling phenomena. Adaptive trabecular bone remodeling is a biological process by which trabecular bone adjusts its structure in response to changing mechanical loads. This is a key mechanism that allows bones to maintain their strength and structural integrity. Trabecular bone is a type of bone found primarily in the ends of long bones, such as the femur and vertebrae. From the mechanical point of view the clue of the remodeling process is minimizing tissue mass and at the same time achieving the highest possible structural stiffness. This process is described by the regulatory model [16–19]. The regulatory model of trabecular bone refers to the mechanisms and processes that govern the remodeling and adaptation of trabecular bone in response to mechanical stimuli by mechanotransduction process. What is also very important, this process takes place only on the surface of the trabecular bone.

The numerical method to solve the optimum design problem is considered already in [20–23] without mathematical background. To this end a new shape functional is defined by

$$J(\Gamma) := \int_{\Gamma} F(\sigma(u) : \varepsilon(u) - \lambda)\,\mathrm{d}\Gamma(x), \tag{14}$$

where F is a given function. This assumption can reflect the idea of homeostasis. The regulatory model presented in Fig. 1 can be described by the relation of the remodeling process to the mechanical stimulation. The main assumption resulting from clinical observation is the existence of a certain mechanical stimulation value λ, characteristic of bone tissue and related to the tissue mechanical parameters, measured with strain energy density (SED). This distinguished value, called the homeostatic stimulation value, defines an ideal state in which there is an ideal balance between resorption and new tissue formation. If this situation occurs, it means that there is no need to modify the amount of tissue at a given location in the structural surface (locally). If, on the other hand, the value of mechanical stimulation from external forces differs from the distinguished value of λ (practically for SED values outside the insensitivity zone), the process of remodeling will caused in different amount of tissue and s is parameter controlling a size of the insensitivity zone. If the excitation is greater than the $\lambda + s$ value, the tissue will be added to the structural surface; if it is less than the $\lambda - s$ value, a small amount of the tissue will be removed. The regulatory model, although not complex, allows for a very good simulation of this behaviour of the bone tissue under load. The insensitivity concept was originally proposed by Carter [24] as an enhancement of the mechanostat theory of Frost [16]. Another name is the lazy zone, which was an expression of the observation that the bone is lazy in response to changes in load. Assuming

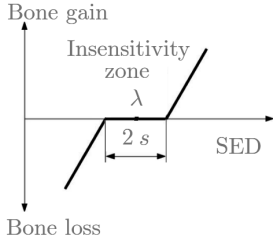

Fig. 1. The regulatory model scheme and the insensitivity zone concept

that the homeostatic SED lambda value is the Lagrangian multiplier from formula (13), one can describe a biomimetic way to achieve stiffest design solution.

The heuristic algorithm is as follows

- it is assumed that the energy density $\sigma(u) : \varepsilon(u)$ has a constant value λ on Γ_v;
- if at a given point on Γ_v this density is greater than $\lambda + s$, then the boundary is moved outside;
- if at a given point on Γ_v this density is smaller than $\lambda - s$, then the boundary is moved inside;
- these steps are repeated until equilibrium is achieved;
- the value of λ is modified if the final design is unsatisfactory;

where s is parameter controlling a size of the insensitivity zone and Γ_v is a part of its boundary subject to modification. The value of λ is unknown. In order to determine it properly, it is necessary to refer to the strength parameters of the material. Such an estimation of the relationship between the condition of constant value of strain energy density on the structure surface and the material strength according to the strength hypotheses criteria will allow for effective use of the method.

4. RELATION BETWEEN HUBER YIELD CRITERION AND ELASTIC ENERGY ON FREE SURFACE

When considering the shape optimization problem consisting in compliance optimization under volume constraint, it is known that if the variable part of the boundary (design boundary) is unloaded, then the elastic energy density on this boundary according to formula (13) is constant.

Knowledge of λ is crucial for the optimization procedure. On the other hand, the structure should satisfy the yield condition, in this case the Huber-Mises-Hencky condition. Hence there arise the following questions:

- What is the relation between the energy density and Huber-Mises-Hencky criterion?
- How to guarantee the structure integrity by setting the appropriate λ?
- What is the best starting λ for launching the optimization process?

It is possible to assume that the variable boundary consists of several smooth patches and consider a point P in the interior of such a patch. Let us attach to the point P a coordinate system with the x_3 axis pointing perpendicularly outside the body and x_1, x_2 plane tangent to the boundary.

Since the surface is free, then

$$\sigma_{3j} = \sigma_{j3} = 0 \quad \text{for} \quad j = 1,2,3. \tag{15}$$

Now by rotating the x_1, x_2 axes around x_3 we may further diagonalize the remaining part of $\boldsymbol{\sigma}$. As a result, the system x_1, x_2, x_3 may be considered as corresponding to principal stresses. Observe that only σ_{11} and σ_{22} may be nonzero.

Invoking the Hooke'e law in the principal stresses coordinates (isotropic material)

$$\varepsilon_{ii} = \frac{1}{E}\left[(1+\nu)\sigma_{ii} - \nu s\right] \quad \text{for} \quad i = 1,2,3, \tag{16}$$

where $s = \sigma_{11} + \sigma_{22} + \sigma_{33}$, it is possible to write down the expression for λ (twice the elastic energy density)

$$\lambda = \frac{1}{E}\left[(1+\nu)(\sigma_{11}^2 + \sigma_{22}^2 + \sigma_{33}^2) - \nu s^2\right] \tag{17}$$

and the reduced stress corresponding to the Huber-Mises-Hencky criterion

$$\sigma_{\text{red}}^2 = \frac{1}{2}\left[(\sigma_{11} - \sigma_{22})^2 + (\sigma_{11} - \sigma_{33})^2 + (\sigma_{22} - \sigma_{33})^2\right]. \tag{18}$$

In general there is no relation between these two quadratic forms in terms of principal stresses, because λ is positive definite, while σ_{red} is not and always vanishes for the body subjected to uniform pressure.

In the situation described above formulas (17), (18) reduce to

$$\lambda = \frac{1}{E}\left[\sigma_{11}^2 + \sigma_{22}^2 - 2\nu\sigma_{11}\sigma_{22}\right] \tag{19}$$

for the energy density and

$$\sigma_{\text{red}}^2 = \sigma_{11}^2 + \sigma_{22}^2 - \sigma_{11}\sigma_{22} \tag{20}$$

for the reduced stress of the Huber-Mises-Hencky criterion. Since $0 < \nu < 1/2$, both quadratic forms are positive definite and may be compared. Denoting $x_1 = \sigma_{11}$, $x_2 = \sigma_{22}$ there are two quadratic forms

$$\lambda E = x_1^2 + x_2^2 - 2\nu x_1 x_2 \tag{21}$$

and

$$\sigma_{\text{red}}^2 = x_1^2 + x_2^2 - x_1 x_2\,. \tag{22}$$

Both forms can be simultaneously diagonalized by substitution

$$x_1 = y_1 - y_2, \qquad x_2 = y_1 + y_2$$

yielding

$$\frac{\lambda E}{2-2\nu} = y_1^2 + \frac{2+2\nu}{2-2\nu}y_2^2 \tag{23}$$

and

$$\sigma_{\text{red}}^2 = y_1^2 + 3y_2^2\,. \tag{24}$$

Observe that

$$0 < \nu < 0.5 \quad \Rightarrow \quad 1 < \frac{2+2\nu}{2-2\nu} < 3.$$

It means that the ellipse corresponding to (24) is slimmer than that corresponding to (23).

The results presented above lead to final conclusions. Let H denote the Huber-Mises-Hencky criterion ellipse together with its interior. Similarly by A_{ext} the smallest ellipse corresponding to (23) containing H is denoted, and by A_{int} the biggest ellipse corresponding to (23) contained in H. It is immediate from the definitions of ellipses that

$$\text{A}_{\text{ext}} \quad \Leftrightarrow \quad \lambda_{\text{ext}} = 2(1-\nu)\frac{\sigma_{\text{red}}^2}{E} \tag{25}$$

and

$$A_{int} \quad \Leftrightarrow \quad \lambda_{int} = \frac{2}{3}(1+\nu)\frac{\sigma_{red}^2}{E}. \tag{26}$$

It is also possible to define the ellipse having the area constituting the average of A_{int} and A_{ext}, for which

$$\lambda_{avr} = \frac{2}{3}(2-\nu)\frac{\sigma_{red}^2}{E}. \tag{27}$$

Figures 2–4 show the layout of these ellipses for different values of ν. The Young modulus is always 210 [GPa], and $\sigma_{red} = 0.5$ [GPa]. The curves have colors: H – green, A_{int} – red, A_{ext} – magenta, A_{avr} – dotted blue.

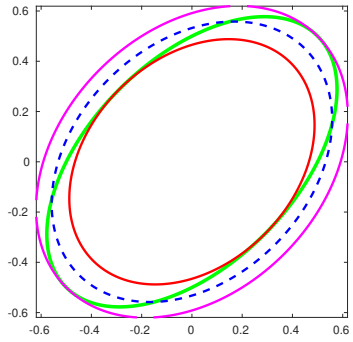

Fig. 2. Huber-Mises-Hencky case – ellipses for $\nu = 0.3$

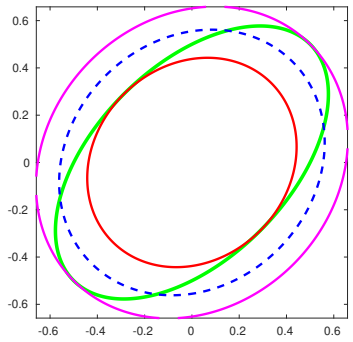

Fig. 3. Huber-Mises-Hencky case – ellipses for $\nu = 0.15$

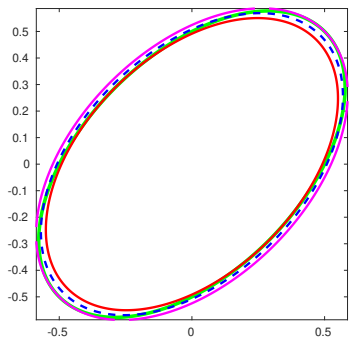

Fig. 4. Huber-Mises-Hencky case – ellipses for $\nu = 0.45$

5. RELATION BETWEEN TRESCA YIELD CRITERION AND ELASTIC ENERGY ON FREE SURFACE

A very similar reasoning may be carried out for the Tresca yield criterion, which has the form

$$\sigma_{red} = \max\left[\,|\,\sigma_{11}-\sigma_{22}\,|, |\,\sigma_{11}-\sigma_{33}\,|, |\,\sigma_{22}-\sigma_{33}\,|\right] \tag{28}$$

where σ_{red} corresponds to twice the maximal shear stress. In our case it reduces to

$$\sigma_{red} = \max\left[\,|\,\sigma_{11}-\sigma_{22}\,|, |\,\sigma_{11}\,|, |\,\sigma_{22}\,|\,\right]. \tag{29}$$

The safe λ (and consequently the energy density) will now be smaller, because the Tresca criterion is stricter than the Huber one. Namely, the safe λ corresponding to the ellipse contained in the Tresca polygon is

$$\lambda_{safe} = \frac{1}{2}(1+\nu)\frac{\sigma_{red}^2}{E}. \tag{30}$$

The outer ellipse is the same as in the Huber case since the Huber ellipse goes through vertices of the polygon.

The best value, λ_{best}, obtained in the same way as formerly reads

$$\lambda_{best} = \frac{1}{4}(5-3\nu)\frac{\sigma_{red}^2}{E}. \tag{31}$$

Again it is smaller. Figures 5–7 show the geometry of the situation for various values of ν.

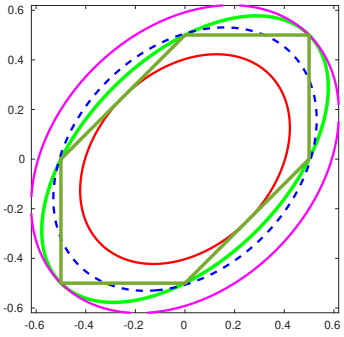

Fig. 5. Tresca case for $\nu = 0.3$

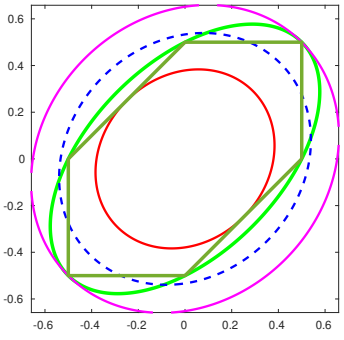

Fig. 6. Tresca case for $\nu = 0.15$

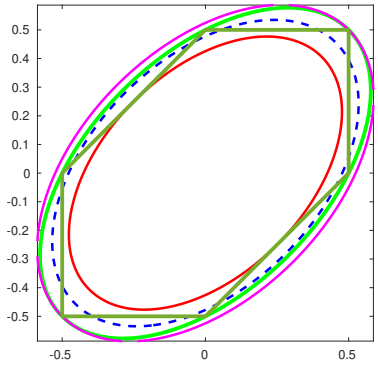

Fig. 7. Tresca case for $\nu = 0.45$

6. REGULARIZATION OF THE OPTIMIZATION METHOD USING THE INSENSITIVITY ZONE

Structural optimization is an excellent way to achieve solutions that are much better than those that are possible using traditional design methods. The design process can be divided into two stages, namely the synthesis stage and the analysis stage. In the synthesis stage, key decisions must be made regarding the shape of the designed structure. This stage is served by topological optimization, which is crucial from the point of view of obtaining a structure with the highest stiffness and minimized mass. Since topological optimization concerns the synthesis stage (at this stage, the spatial shape of the structure is sought and is not known), it differs from shape optimization and size optimization. Also, the developed tools and methods used to perform topological optimization are specific and different from other structural optimization methods. In the group of various approaches to the topology optimization problem, the most popular is the SIMP (Solid isotropic material with penalization) method [25–29]. It has practically dominated commercial software and is dominant in industrial practice [30–33]. Since the problem of stiffest design, the goal of the topology optimization algorithm (compliance minimization) has no solution without additional assumptions, usually the volume of the material in the design domain is limited. But this is a fundamental problem in this approach, because there can be no guidelines on how to choose the value of the volume constraint in any domain. In the approach described in the paper, the design paradigm is different and refers to the Lagrange multiplier, and as shown in the previous chapters, further to the strength properties of the material. Instead of the volume constraint, the Lagrange multiplier is assumed (according to strength hypothesis) to have a constant value during the whole optimization procedure. The relationship between the Lagrange multiplier and the volume constraint has been described in many papers on topological optimization methods [34, 35]. In the paper [35] the authors discuss the problem of designing an optimal shape and note that increasing the Lagrange multiplier leads to a decrease in the weight of the solution. In a sense, this corresponds to the relationship of the multiplier with material properties postulated in the paper. The relation of the adopted value of the Lagrange multiplier to the obtained volume of the optimal solution also depends on other parameters of the optimization procedure itself. It is usually assumed [28, 36] that the material volume is a monotonically decreasing function of the Lagrange multiplier. Therefore, in the classical approach like SIMP method, the Lagrange multiplier is treated only as a coefficient that must be found to satisfy the volume constraint. Experience shows that the application of existing procedures leads to reasonable results, although for example in [36, 37] it was stated that there is no rigorous proof of its existence for each of the volume constraints. In the approach presented in the paper, the optimization method is based on the regulatory model of trabecular bone remodeling. An important element of the concept of building a system for the biomimetic structural optimization method is the notion of insensitivity zone. The connection between observations of nature and the optimization problem, especially in relation to bone remodeling and to apply the bio-mechanical observations and models to the structural optimization issues can be found in various works presenting different approaches [38, 39]. In the latter paper, the concept of the insensitive zone was used in the description of the dynamical system and the role of the insensitivity zone itself in the dynamical system approach to optimization was indicated. However, the formulations used are based on the assumption of density formulation, indicating similarities between the theory of bone remodeling and the density formulation of topology optimization. In the approach presented in the paper, there are no assumptions regarding the use of artificial material in the optimization process. Each iteration corresponds to a functional configuration modeled from a specific material with specific strength properties. It is in the context of the value of the Lagrangian multiplier adopted in the model by using insensitivity zone, rather than a single value, that regularization will be applied in the biomimetic optimization method. The use of this concept allows for regularization without focusing on the existence of the Lagrange multiplier correspondence to the volume constraint. In fact, bone remodeling continues uninterrupted, regardless of whether the local bone loads are within the insensitivity zone or not. In addition to the load itself (measured by the SED value), the way in which the bone is loaded is also important. And this is also why the existence of the insensitivity zone in bone remodeling models is essential. It allows for the consideration of the influence of many cases of loading of the bone structure during daily activity, and bone remodeling leads to the evolution of the structure reflecting the recorded mechanical stimulation. Although this is a very interesting area of research [21, 40], for the moment we will focus on defining the parameters characterizing the insensitive zone with reference to the considerations presented in the above sections concerning the relationship between the value of the Lagrange multiplier and the limit stresses resulting from the strength hypothesis. It is therefore necessary to find a way to determine the lower and upper limits of the insensitivity zone and to develop heuristics useful in numerical calculations.

7. ACQUIRED HEURISTICS AND COMPUTATION STRATEGY

To carry out the biomimetic structural optimization simulation it is necessary to combine two areas – numerical simulation of deformation of the structure under load and structural evolution. The finite element method is used, FrontISTR [41,42] was selected for this purpose.

The more difficult task is to plan how to reflect the evolution of the structure. Complete flow of the system is presented in Fig. 8. Based on previous experience [43], it was decided to build separate computational meshes for each simulation step. Input finite element mesh, provided in STL format, is sliced into a set of two-dimensional images containing the cross-sections of the input data. Set of slices is the primary representation of data in the structural optimization system. Before volumetric mesh generation, data is first discretized to reduce scale of the problem and thus reduce the mesh size. This enables storing high-resolution two-dimensional slices while performing stress simulation on data of reduced scale for faster computation. Discretized data is used to build volumetric mesh, by creating mesh cells by spanning tetragonal elements between adjacent slices, as shown in Fig. 9. Comparison of input mesh and mesh recreated from discretized data is shown in Fig. 10. Resulting mesh, free of topological defects, is used as an input for stress simulation. According to the remodeling scenario described by the regulatory model, depending on the calculated value of the energy density, the surface of the structure is modified by adding or removing material on its surface. In the most basic version of the remodeling algorithm two threshold energy values are defined – high and low. If material is present in an area with energy below the low value, it is removed if energy is above the high value, material is added. Result of 5 iterations of the algorithm is shown in Fig. 11.

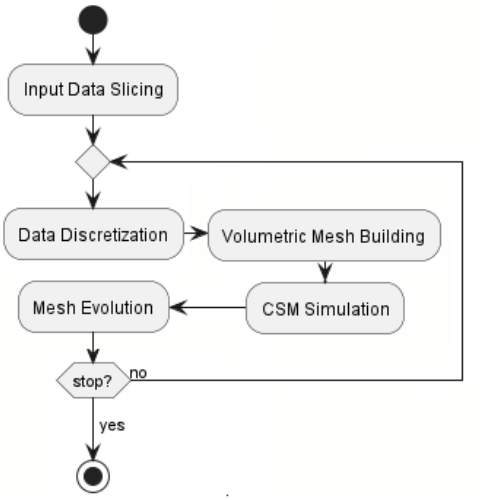

Fig. 8. Activity diagram for the structural optimization system. Input data is sliced into a collection of two-dimensional images. In each iteration discretization of data is performed followed by volumetric mesh building. Created mesh is an input for stress simulation, which is used as input for mesh evolution

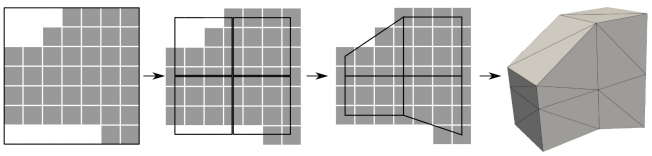

Fig. 9. Data discretisation and volumetric mesh building steps performed for sample data. Input data is approximated by low-scale polygons which are used to build volumetric mesh

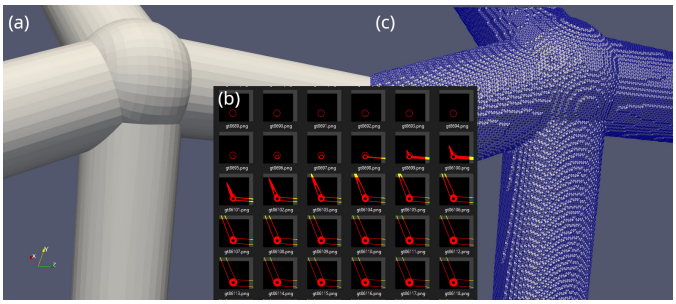

Fig. 10. (a) Sample input data – structural node connecting four beams; (b) Input data sliced into a collection of two-dimensional images; (c) Volumetric mesh reconstructed from slices

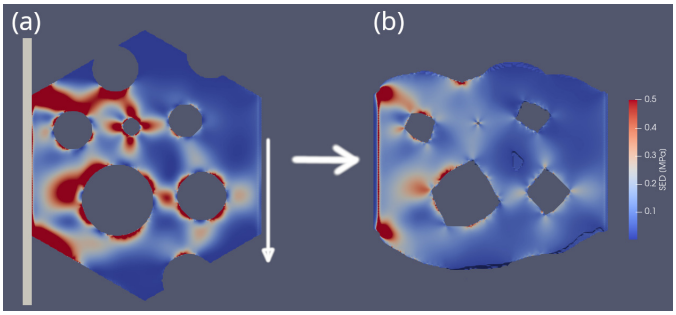

Fig. 11. Example of mesh evolution: (a) Input data is a structure with random holes, supported on the left side with sheer force applied on the right side; (b) Structure after 5 steps of evolution. Material grew in areas with high energy and was removed where energy was low

In practical applications the simple evolution algorithm, based on two fixed thresholds, has numerous issues caused by imperfections of underlying representation. To demonstrate issues caused by loss of resolution introduced by data discretization consider four identical bars with rectangular cross sections. Each bar is made of aluminum ($\nu = 0.33$, $E = 70$ MPa) and has length of 300 mm and a side of 10 mm. Slicing is performed along the X axis of coordinate systems (each slice represents a cross-section of input data and YZ plane). First bar, named baseline, BL is aligned along the X axis. Second and third, Y15 and Y30, are BL rotated 15 and 30 degrees along the Y axis, respectively. Fourth, YZ, is rotated along the Y axis by 15 degrees and then rotated along the Z axis by 15 degrees. Each bar was supported from one side and stretched along its axis with force of 50 kN and simulation using the structural optimization system was performed – input data was sliced and volumetric mesh was reconstructed and used for simulation. Results are shown in Fig. 12. Stress distribution on the surface of each test case was calculated and is shown in Fig. 13. Baseline test case (BL),

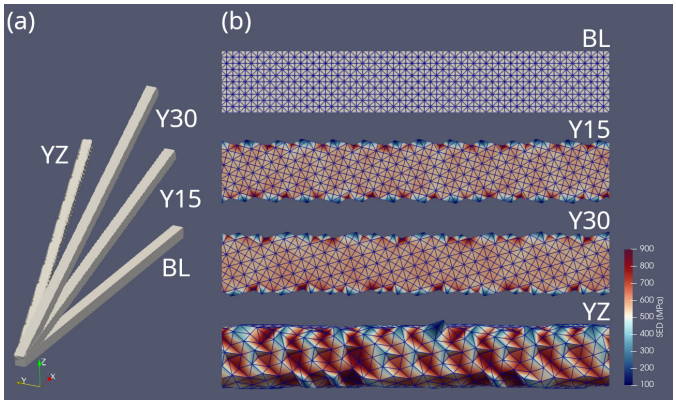

Fig. 12. (a) Four bars, superimposed, used to demonstrate the impact of volumetric mesh imperfections on the simulation; (b) Fragment of each bar next to each other. Baseline (BL) bar, aligned to the slicing axis, has uniform energy distribution on the surface. Other three bars, due to surface imperfections, exhibit surface energy variations

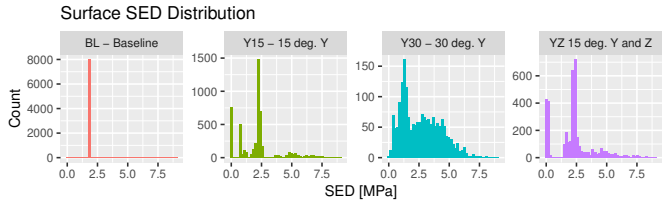

Fig. 13. Distribution of strain energy density on the surface on four bars shown in Fig. 12. The baseline bar has uniform energy distribution. All other test cases have energy variations

which has sides parallel to slicing axis, can be perfectly represented in the reconstructed mesh. This leads to uniform energy distribution on the surface. Other three test cases have surfaces approximated by finite elements mesh with different degrees of accuracy. This leads to non-uniform distribution with visible notches, where energy is concentrated, and areas with increased cross-section where energy is lower. The evolution algorithm based on fixed thresholds does not perform well for such data. Surface imperfections lead to oscillations, when the algorithm adds and removes material in the same area due to inability to even out surface energy. To mitigate this effect a heuristic approach with dynamic thresholds is used.

Structural optimization performed by the algorithm is local search that starting from the initial configuration performs space search of all possible shapes by evolving mesh according to strain energy distribution on the surface. The goal of optimization is to fit the distribution of energy on the structural surface between two thresholds defining the insensitive zone. The initial version used fixed insensitive zone. For the upper value of insensitive zone λ_{avr} calculated using (27) was used, for lower $0.5\lambda_{\text{avr}}$. During algorithm development and testing, the following numerous observations were made, which lead to definition of heuristic optimization algorithm.

It is not desirable to narrow the insensitive zone as much as possible to concentrate SED distribution because system with too narrow thresholds has tendency to enter oscillations. Oscillations are caused by two distinct phenomena. One class of oscillations appears in areas where very fine structure of beam elements, as predicted by theoretical models, cannot be realized by the finite elements model. Those oscillations are manifested as a porous structure that changes each step. This kind of behavior can be described as 'harmless' – it does not affect the optimized structure as a whole and appears only in areas between well defined and stable features. Second group of oscillations is caused by inability to represent optimal size of beam-like element using finite elements mesh. In this scenario system changes between structure with excess energy and structure with energy too low, below the lower threshold and is unable to fit the whole surface energy distribution inside the insensitive zone. This effect is additionally magnified by surface imperfections, presented earlier. This group of oscillations can lead to change of topology by breaking beam element, which in extreme cases can lead to the collapse of structure. This in turn causes rapid degradation of quality of the solution and algorithm starts pursuing different optimum, usually ending up with worse quality of the final solution.

Increasing resolution of the finite mesh does not solve the issue with destructive oscillations. The finite element size is an input parameter to the system and decreasing the element size leads to the increase in a resolution of the finite elements mesh. Increase in resolution does not mitigate problems with oscillations as a higher resolution leads to a different topology, where a finer structure can be realized. This, in turn, brings back the oscillation issue.

The use of a wide insensitive zone leads to decreased amount of oscillations by allowing a wider variety of sizes that can be 'fit' inside. Wide insensitive zone leads to an increased set of solutions that are considered optimal by the system. This allows definition of secondary quality measures to compare optimal solutions. Three secondary measures are considered: maximum displacement, volume and average surface SED. Maximum deflection is maximum displacement, calculated during simulation. Volume is the total volume of the finite elements mesh. Volume, not mass, is used because it does not require density as an additional system input. Average surface SED is average value of strain energy density on the surface of optimized object. Average surface SED should be as high as possible, because structural optimization should get surface energy density distribution as close to the upper threshold value as possible. Observation of behavior of surface SED distribution and average value in particular allows us to better understand and fine tune the algorithm. From the practical perspective average surface SED is irrelevant. The two other measures are very easy to measure in the implementation of the optimized structure. Maximum displacement and volume are not correlated – all solutions on the Pareto front are optimal according to secondary criteria. In scenarios where initial state has parts with surface energy significantly below the lower threshold, it is beneficial to slow down initial removal process. For the parts with high aspect ratio (i.e., flat bar) material removal, which behaves in this case similar to morphological dilation, can remove the whole structure. If the process is manually slowed down by decreasing the initial value of the lower threshold for few iterations the

structure can be refined into a part with higher energy density on the surface and optimization process will continue.

It was observed that wide insensitive zone leads to suboptimal solutions in cases where the initial state has strain energy density above the upper threshold, which results in initial material removal. This observation is counter-intuitive, as approaching insensitive zone from the higher value should lead to solution with a higher average surface SED than approaching the same zone from the lower values. Higher average SED should, in turn, lead to better secondary measures of obtained optimum. Performed tests lead to observation that approaching insensitive zone from the high average surface SED values makes optimization process susceptible to local optima and local search used is not able to leave them.

The stop criterion, defined as fitting the whole energy into the insensitive zone is, in practice, rarely met and instead optimization runs for set amount of iteration. Upper value of the insensitive zone is derived from the von Mises yield criterion hence the final solution must be free of elements exceeding this threshold. Elements with energy below the lower threshold are allowed.

To overcome described issues the system was modified and fixed thresholds were replaced with a heuristic algorithm utilizing dynamic threshold values. Proposed approach consists of four steps and instead of using stop criteria it works with a fixed number of steps.

Used heuristic is an attempt to create universal optimization algorithm which contains all practical experience gathered during testing in a closed form solution. This allows performing structural optimization with hands off approach, that is flexible enough to work with different input data. Proposed heuristic uses dynamic insensitive zone that depends on input parameters and surface SED distribution. Algorithm uses following parameters:

- number of iterations, n – total number of optimization iterations to perform,
- material yield strength, σ_{red}, used internally to calculate λ_{avr} using formula (27) which is used as an upper threshold of the insensitive zone.
- initial upper threshold reduction, α – value between $(0, 1]$ used to decrease initial value of the upper threshold,
- initial and final percentile of surface SED distribution, $\beta_{\text{init}}, \beta$ – algorithm calculated dynamic value of the lower threshold dynamically each step as a requested percentile of surface SED distribution. Two parameters are provided, initial and target, as percentile varies with the optimization progress.

If at any point heuristic returns insensitive zone with lower threshold value above higher, the lower threshold is set to 50% of the higher value instead.

The first phase of optimization is performed for the first 25% of optimization steps and uses $upper = \alpha\lambda_{\text{avr}}$ and $lower = P(SED;\beta_{\text{init}})$ for insensitive zone boundaries, where $P(SED;p)$ returns value of given percentile p of the distribution of surface SED. This phase has two main goals. The upper threshold is deliberately lower to promote the overgrowth of the optimized structure and to make sure the final insensitive zone is approached 'from the top' as it was observed it leads to better optimization results. Percentile, used to dynamically determine the lower threshold, is used to slow down material removal rate and parameter with value of x can be informally read as 'at most x% of elements can be removed in a single step.'

Second phase happens for the 50%n steps of iteration, so ends at the 75%n of total optimization steps. During the start of this phase lower and upper thresholds are calculated using formulas from the previous step. At the end $upper = \lambda_{\text{avr}}$ and $lower = P(SED;\beta)$. For the steps in between linear regression is used to calculate threshold values using step number. Optimization gradually reaches the target insensitive zone. β value is higher than $beta_{\text{init}}$ – initially slow rate of material removal has to be increased to make insensitive zone narrower, hence increasing quality of the final solution.

Third phase happens between steps 75%n and $n-5$ and the final values from the previous phase, $upper = \lambda_{\text{avr}}$ and $lower = P(SED;\beta)$ are sustained. The final solution is refined during this phase.

The last phase is executed for exactly 5 iterations and during it the lower threshold is decreased down to zero. Any remaining oscillations are damped and with only material increase available we guarantee all surface SED will be below the critical value λ_{avr} thus the von Mises yield criterion will not be exceeded under designed load.

To demonstrate algorithm operation optimization was performed on a 200 mm aluminum rod ($\nu = 0.33$, $E = 70$ MPa) element attached to a cylindrical support with a diameter of 20 mm, stressed using force of 5 kN. Tensile strength $\sigma_{\text{red}} = 100$ MPa. Three structural optimizations were performed, each using 250 iterations. First optimization was performed with fixed insensitive zone. Second used heuristic approach with parameters $\alpha = 0.25$, $\beta_{\text{init}} = 5\%$, $\beta = 15\%$ and third run was using heuristic approach with parameters $\alpha = 0.25$, $\beta_{\text{init}} = 5\%$, $\beta = 25\%$. Input shape and results of optimization are shown in Fig. 14. Each optimization resulted in a structure with surface SED for all optimized elements inside the lazy zone. To compare those results secondary measures were calculated, shown in Table 1. Plots of changes of secondary measures, with additional von Mises stress are shown in Fig. 15.

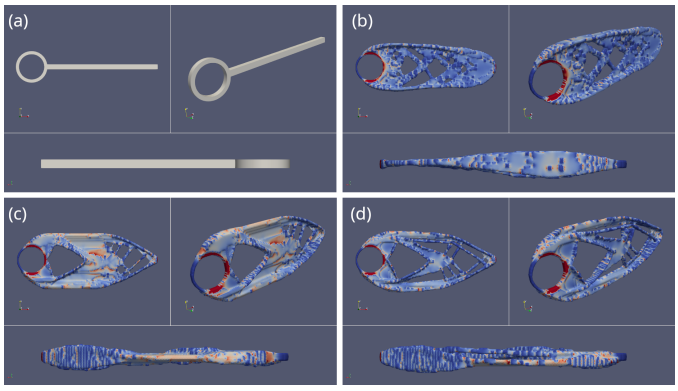

Fig. 14. (a) Input data for the sample structural optimization problem. Rod is attached to cylindrical support and stressed on the far end. (b) Result of optimization using fixed insensitive zone. (c, d) Result of optimization using heuristic approach with different parameters

Table 1
Secondary quality measures for three optimizations for the sample problem

Case	Volume [mm^3]	Max.-Displ. [mm]
Baseline	77753.06	0.000928
Candidate 1	65917.80	0.001060
Candidate 2	73790.17	0.000947

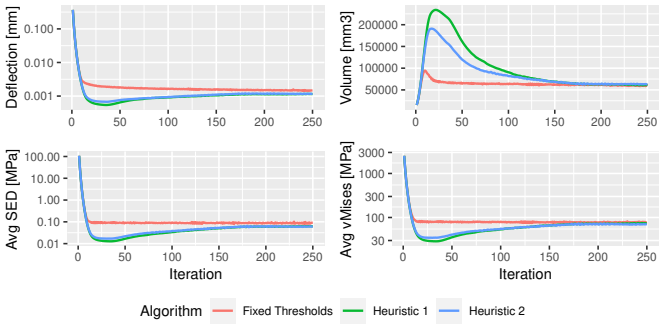

Fig. 15. Three structural optimizations with different heuristics: Baseline: fixed insensitive zone, Candidate 1 heuristic: parameters values $\alpha = 0.25$, $\beta_{\text{init}} = 5\%$, $\beta = 15\%$ and Candidate 2 heuristic: parameters values $\alpha = 0.25$, $\beta_{\text{init}} = 5\%$, $\beta = 25\%$

8. NUMERICAL EXAMPLES

The presented example will be the cantilever beam in bending, in which all nodes of one edge could be fixed (clamped wall) and the bending force is applied to the middle of the opposite edge. Simulation was run for two different materials – steel and aluminum, each using two different starting configurations. First starting configuration was full domain, second was T-shaped element. Data was selected to allow comparison with other optimization techniques described in literature [44].

Despite optimization system being designed to work with three-dimensional models, the optimization domain size was restricted in one dimension to emulate two-dimensional optimization. This restricted dimension is arbitrary referred to as a model thickness. Thickness size was selected to ensure model, used for the simulation, had exactly five integration points along the restricted dimension. This ensured both good numerical solutions and uniform model thickness. Decrease of restricted dimension would decrease amount of integration point affecting quality of the solution, increasing would allow algorithm to vary model thickness, making it no longer two-dimensional.

All four optimizations were run using the same heuristic settings, shown in Table 2. Results are shown in Fig. 16 and optimization process is shown in Fig. 17. In all four cases optimization resulted in an optimal shape, with a different topology and thickness for steel and aluminum. The same topology was achieved for optimization starting from beam and full domain.

Table 2
Optimization parameters used in all four optimizations

Parameter	Symbol	Value
Steel tensile strength	σ_{red}	300 MPa
Steel lazy zone upper value	λ_{avr}	0.510 MPa
Aluminum tensile strength	σ_{red}	100 MPa
Aluminum lazy zone upper value	λ_{avr}	0.160 MPa
Iterations	n	250
Initial upper threshold reduction	α	0.25
Initial lower threshold percentile	β_{init}	5%
Final lower threshold percentile	β	15%

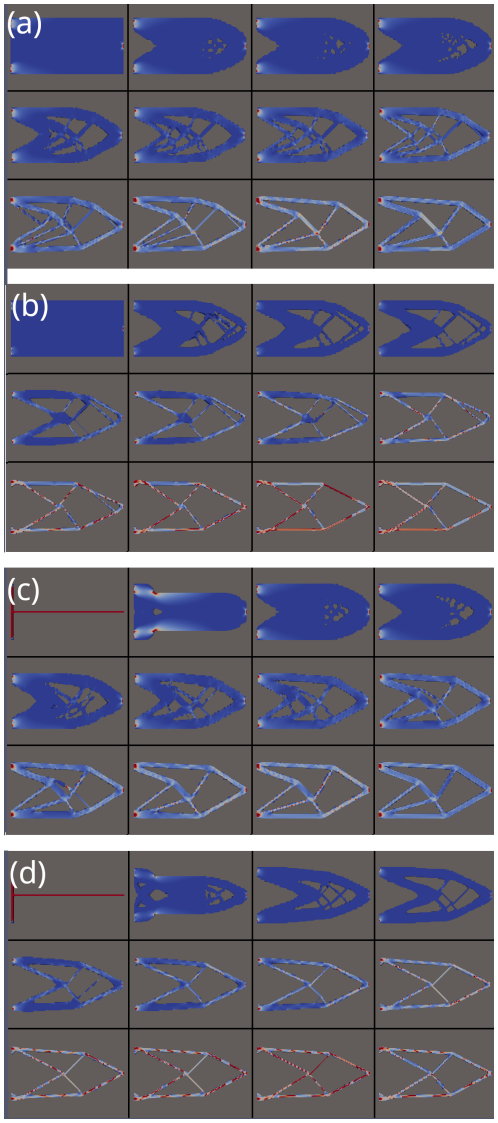

Fig. 16. Results of selected steps of the optimization process, showing evolution of topology and the final solution of all four test cases. (a) Aluminum, starting from a full domain. (b) Steel, starting from a full domain. (c) Aluminum, starting from a bar. (d) Steel, starting from a bar

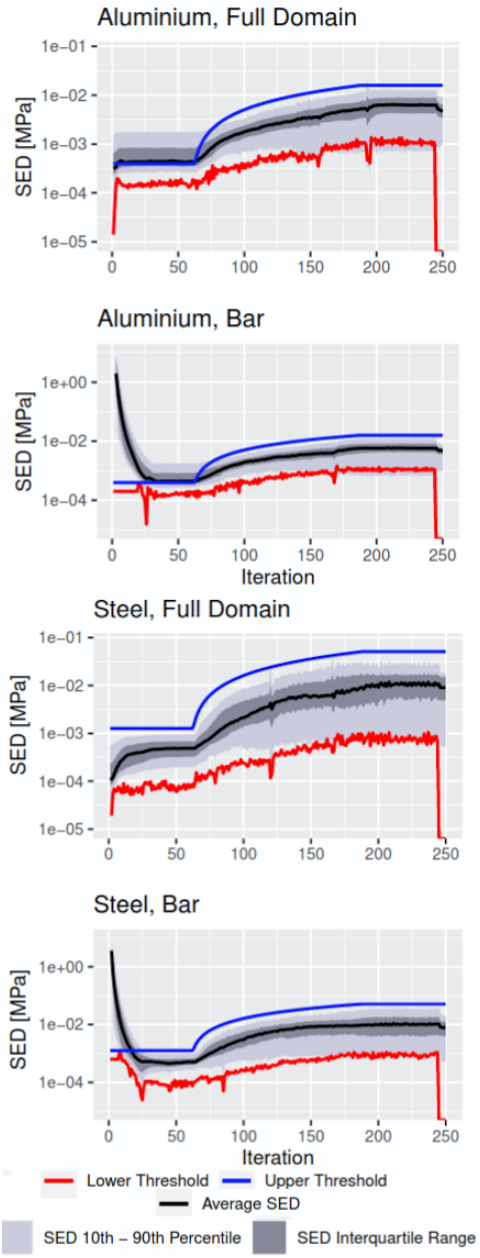

Fig. 17. Plots for all four test cases showing changes in SED on the structural surface during the optimization process. Each plot shows four distinct phases of the heuristic algorithm: initial phase, where structure growth is promoted, transition phase, where parameters move towards target values, stable phase, where the final structure forms and the final refinement

9. CONCLUSIONS

The paper presents a new approach to shape optimization. The main issue is the theoretical result-based assumption of equivalence of energy minimization in the whole volume with a configuration in which the energy density on the surface is constant. In this way, a biomimetic approach can be used, which is in turn based on observation of the remodeling phenomenon of the trabecular bone. The important thing, as presented in the paper, is to indicate how to determine the value of the energy density on the structural surface. Naturally, this value should be based on strength hypotheses, because the material properties determine the acceptable load on any part of the structure. The presented discussion allows, after assuming the strength hypothesis, to solve this problem. The paper discusses two strength hypotheses, the Huber-Mises-Hencky hypothesis and the Tresca hypothesis, and for these hypotheses presents formulas combining the reduced stress calculated according to the hypothesis and the value of the energy density on the surface of the optimized structure. Examples using the Huber-Mises-Hencky hypothesis are presented. In this way, a procedure was developed that allows shape optimization without the volume condition, but instead with the assumption of material strength parameters. From the point of view of engineering practice this gives a much better solution than guessing the correct first the domain and second the volume constraint, which in addition has the disadvantage that in view of the nonlinearity of the solution space there is no certainty of achieving the correct solution. Two more things should be noted: – the postulate of correlating the value of the energy density on the surface with the properties of the material applies to the target configuration, – for the proper use of the features of such an approach (for example, solving the problem of multiple load cases), it is necessary to determine the location and size of the insensitivity zone. The approach presented in the paper therefore, requires the development of heuristics that allow achieving the assumed goal in the numerical procedure regardless of the initial configuration. Such heuristics have been developed and operate independently of the starting point, as shown by the numerical examples. The procedure works stably and has been programmed with the assumption of using parallel processing, which allows for thinking about the industrial application of the developed programs. It should be emphasized that without the need for filtering and the use of artificial material definition, the proposed approach leads directly to mass minimization. Additionally, the problem of many load cases and changes in the shape and topology of the structure associated with the change of the used material are an inherent feature of the presented approach. The final result is a geometric model that can be produced using additive methods [45]. Also in this context, the presented method is a promising direction for further research.

REFERENCES

[1] P. Plotnikov and J. Sokołowski, "Geometric aspects of shape optimization," *J. Geom. Anal.*, vol. 33, no. 7, Paper No. 206, pp. 1–57, 2023.

[2] W. Wang, D. Munro, C.C.L. Wang, F. van Keulen, and J. Wu, "Space-time topology optimization for additive manufacturing," *Struct. Multidiscip. Optim.*, vol. 61, no. 1, pp. 1–18, 2020, doi: 10.1007/s00158-019-02420-6.

[3] Y. Saadlaoui, J.-L. Milan, J.-M. Rossi and P. Chabrand, "Topology optimization and additive manufacturing: Comparison of conception methods using industrial codes," *J. Manuf. Syst.*, vol. 43, pp. 178–186, 2017, doi: 10.1016/j.jmsy.2017.03.006.

[4] J. Zhu, H. Zhou, C. Wang, L. Zhou, S. Yuan, and W. Zhang, "A review of topology optimization for additive manufacturing: Status and challenges," *Chin. J. Aeronaut.*, vol. 34, no. 1, pp. 9–110, 2021, doi: 10.1016/j.cja.2020.09.020.

[5] A.P. Wierzbicki and S. Kurcyusz, "Projection on a cone, penalty functionals and duality theory for problems with inequaltity constraints in Hilbert space," *SIAM J. Control Optim.*, vol. 15, no. 1, pp. 25–56, 1977.

[6] A.P. Wierzbicki and S. Kurcyusz, "Projection on a cone and generalized penalty functionals for problems with constraints in Hilbert space," *Bull. Pol. Acad. Sci. Tech. Sci.*, vol. 22, pp. 983–988, 1974.

[7] M.T. Huber, "Specific strain work as a measure of material effort," *Czasopismo Techniczne, Lwów, Organ Towarzystwa Politechnicznego we Lwowie*, vol. 22, pp. 34–40, 49–50, 61–62, 80–81, 1904.

[8] R. von Mises, "Mechanik der festen Körper im plastisch-deformablen Zustand," *Nachrichten von der Gesellschaft der Wissenschaften zu Göttingen. Mathematisch-Physikalische Klasse*, vol. 1, pp. 582–592, 1913.

[9] H. Tresca, "Mémoire sur l'écoulement des corps solides soumis à de fortes pressions," *C.R. Acad. Sci. Paris*, vol. 59, p. 754, 1864.

[10] A. Cunha, Y. Yanik, C. Olivieri, and S. da Silva, "Tresca vs. von Mises: Which Failure Criterion is MoreConservative in a Probabilistic Context?," *J. Appl. Mech.*, vol. 91, no. 11, 111008, 2024, doi: 10.1115/1.4063894.

[11] Z. Wasiutyński, "On the congruency of the forming according to the minimum potential energy with that according to equal strength," *Bull. de l'Academie Polonaisedes Sciences, Serie des Sciences Techniques*, vol. 8, no. 6, pp. 259–268, 1960.

[12] P. Pedersen, *Optimal Designs – Structures and Materials – Problems and Tools*, ISBN 87-90416-06-6, 2003.

[13] M. Mrzygłód, "Multi-constrained topology optimization using constant criterion surface algorithm," *Bull. Pol. Acad. Sci. Tech. Sci.*, vol. 60, no. 2, pp. 229–236, 2012, doi: 10.2478/v10175-012-0030-9.

[14] M. Nowak and A. Boguszewski, "Topology optimization without volume constraint – the new paradigm for lightweight design," *Bull. Pol. Acad. Sci. Tech. Sci.*, vol. 69, no. 4, p. e137732, 2021, doi: 10.24425/bpasts.2021.137732.

[15] J. Wolff, *Das Gesetz der Transformation der Knochen*, Hirschwald, Berlin, 1892.

[16] H.M. Frost, *The Laws of Bone Structure*, C.C. Thomas, Springfield, 1964.

[17] R. Huiskes, H. Weinans, H.J. Grootenboer, M. Dalstra, B. Fudala, and T.J. Slooff, "Adaptive bone-remodeling theory applied to prosthetic-design analysis," *J. Biomech.*, vol. 20, no. 11-12, pp. 1135–1150, 1987, doi: 10.1016/0021-9290(87)90030-3.

[18] R. Huiskes, R. Ruimerman, G.H. van Lenthe, and J.D. Janssen, "Effects of mechanical forces on maintenance and adaptation of form in trabecular bone," *Nature*, vol. 404, pp. 704–706, 2000.

[19] I. Goda, J.F. Ganghoffer, S. Czarnecki, P. Wawruch and T. Lewinski, "Optimal internal architectures of femoral bone based on relaxation by homogenization and isotropic material design," *Mech. Res. Comm.*, vol. 76, pp. 64–71, 2016.

[20] M. Nowak, J. Sokołowski, and A. Żochowski, "Justification of a certain algorithm for shape optimization in 3D elasticity," *Struct. Multidiscip. Optim.*, vol. 57, no. 2, pp. 721–734, 2018, doi: 10.1007/s00158-017-1780-7.

[21] M. Nowak, J. Sokołowski, and A. Żochowski, "Biomimetic Approach to Compliance Optimization and Multiple Load Cases," *J. Optim. Theory Appl.*, vol. 184, pp. 210–225, 2020, doi: 10.1007/s10957-019-01502-1.

[22] I. Goda, J.F. Ganghoffer, S. Czarnecki, R. Czubacki, and P. Wawruch, "Topology optimization of bone using cubic material design and evolutionary methods based on internal remodeling," *Mech. Res. Commun.*, vol. 95, pp. 52–60, 2019.

[23] J.F. Ganghoffer and J. Sokolowski, "A micromechanical approach to volumetric and surface growth in the framework of shape optimization," *Int. J. Eng. Sci.*, vol. 74, pp. 207–226, 2014.

[24] D.R. Carter, "Mechanical loading histories and cortical bone remodeling," *Calcif. Tissue Int.*, vol. 36 (Suppl. 1), pp. S19–S24, 1984.

[25] M. Bendsoe and O. Sigmund, *Topology optimization. Theory, methods and applications*, Berlin Heidelberg New York, Springer, 2003, doi: 10.1007/978-3-662-05086-6.

[26] M. Bendsoe and N. Kikuchi, "Generating optimal topologies in structural design using a homogenization method," *Comput. Methods Appl. Mech. Eng.*, vol. 71, pp. 197–224, 1988.

[27] O. Sigmund, *On the Optimality of Bone Microstructure. Synthesis in Bio Solid Mechanics*, Kluwer, pp. 221–234, 1999.

[28] O. Sigmund, "A 99 line topology optimization code written in Matlab," *Struct. Multidiscip. Optim.*, vol. 21, no. 2, pp. 120–127, 2001, doi: 10.1007/s001580050176.

[29] O. Sigmund and K. Maute, "Topology optimization approaches," *Struct. Multidiscip. Optim.*, vol. 48, pp. 1031–1055, 2013, doi: 10.1007/s00158-013-0978-6.

[30] L. Krog, A. Tucker, M. Kemp, and R. Boyd, "Topology optimization of aircraft wing box ribs," *AIAA Paper, 10th AIAA/ISSMO Multidisciplinary Analysis and Optimization Conference, Albany, New York*, 2004, doi: 10.2514/6.2004-4481.

[31] Z. Luo, J. Yang, and L. Chen, "A new procedure for aerodynamic missile designs using topological optimization approach of continuum structures," *Aerospace Sci. Tech.*, vol. 10, no. 5, pp. 364–373, 2006, doi: 10.1016/j.ast.2005.12.006.

[32] Z. Ming and R. Fleury, "Fail-safe topology optimization," *Struct. Multidiscip. Optim.*, vol. 54, no. 5, pp. 1225–1243, 2016, doi: 10.1007/s00158-016-1507-1.

[33] M. Zhou, J. Alexandersen, O. Sigmund, and C.B.W. Pedersen, "Industrial application of topology optimization for combined conductive and convective heat transfer problems," *Struct. Multidiscip. Optim.*, vol. 54, no. 4, pp. 1045–1060, 2016, doi: 10.1007/s00158-016-1433-2.

[34] G. Allaire, L. Cavallina, N. Miyake, T. Oka, and T. Yachimura, "The homogenization method for topology optimization of structures: old and new," *Interdiscip. Inf. Sci.*, vol. 25, no. 2, pp. 75–146, 209, doi: 10.4036/iis.2019.B.01.

[35] G. Allaire and R.V. Kohn, "Topology Optimization and Optimal Shape Design Using Homogenization," M. Bendsoe, C. Soares, Eds., *Topology Design of Structures. NATO ASI Series – Series E: Applied Sciences*, vol. 227, pp. 207–218, 1993, doi: 10.1007/978-94-011-1804-0_14.

[36] G. Allaire, *Shape Optimization by the Homogenization Method*, ISBN 978-1-4684-9286-6, Springer, 2002, doi: 10.1007/978-1-4684-9286-6.

[37] G. Allaire, E. Bonnetier, G. Francfort, and F. Jouve, "Shape optimization by the homogenization method," *Numerische Mathematik*, vol. 76, no. 1, pp. 27–68, 1997, doi: 10.1007/s002110050253.

[38] E. Nutu, "Interpretation of parameters in strain energy density bone adaptation equation when applied to topology optimization of inert structures," *Mechanika*, vol. 21, no. 6, pp. 443–449, 2015.

[39] A. Klarbring and B. Torstenfelt, "Lazy zone bone remodelling theory and its relation to topology optimization," *Ann. Solid Struct. Mech.*, vol. 4, no. 1, pp. 25–32, 2012.

[40] M. Nowak, "New Aspects of the Trabecular Bone Remodeling Regulatory Model – Two Postulates Based on Shape Optimization Studies," *Developments and Novel Approaches in Biomechanics and Metamaterials. Advanced Structured Materials*, vol 132, Springer, pp. 97–105, 2020.

[41] R. Aoyagi, R. Imai, J. Rutqvist, H. Kobayashi, O. Kitamura, and N. Goto, "Development of TOUGH-FrontISTR, a numerical simulator for environmental impact assessment of CO_2 geological storage," *Energy Procedia*, vol. 37, pp. 3655–3662, 2013, doi: 10.1016/j.egypro.2013.06.259.

[42] FrontISTR ver. 5.6, Technical report, https://manual.frontistr.com/en/, Accessed: 2025-03-11

[43] M. Nowak, "Structural optimization system based on trabecular bone surface adaptation," *Struct. Multidiscip. Optim.*, vol. 32, no. 3, pp. 241–251, 2006, doi: 10.1007/s00158-006-0027-9.

[44] W. Bremicker, M. Chirehdast, N. Kikuchi, and P.V. Papalambros, "Integrated topology and shape optimization in structural design," *J. Struct. Mech.*, vol. 19, no. 4, pp. 551–587, 1991.

[45] J. Polak and M. Nowak, "From Structural Optimization Results to Parametric CAD Modeling – Automated, Skeletonization-Based Truss Recognition," *Appl. Sci.*, vol. 13, no. 9, 2023, doi: 10.3390/app13095670.